Journal of Biomolecular NMR, 9 (1997) 63–78
ESCOM

J-Bio NMR 409

Backbone dynamics of proteins derived from carbonyl carbon relaxation times at 500, 600 and 800 MHz: Application to ribonuclease T1

Jan Engelke and Heinz Rüterjans*

Institut für Biophysikalische Chemie der Johann Wolfgang Goethe Universität Frankfurt am Main, Biozentrum N230, Marie Curie Strasse 9, D-60439 Frankfurt am Main, Germany

Received 3 June 1996
Accepted 22 October 1996

Keywords: Protein dynamics; ^{13}C relaxation times; Spectral density function mapping; Conformational exchange; Order parameter; Ribonuclease T1

Summary

The backbone dynamics of uniformly $^{13}C/^{15}N$-enriched ribonuclease T1 have been investigated using carbonyl carbon relaxation times recorded at three different spectrometer frequencies. Pulse sequences for the determination of the longitudinal (T_1) and transverse (T_2) relaxation times are presented. The relaxation behaviour was analysed in terms of a multispin system. Although the chemical shift anisotropy relaxation mechanism dominates at high magnetic field strength, the contributions of the dipole–dipole interactions and the cross-correlation between these two relaxation mechanisms have also been considered. Information about internal motions has been extracted from the relaxation data using the model-free approach of Lipari and Szabo in order to determine order parameters (S^2) and effective internal correlation times (τ_i). Using a relatively simple relation between the measured relaxation rates and the spectral density function, an analytical expression for the microdynamical parameters in dependence of T_1 and T_2 has been derived. The spectral density mapping technique has been applied in order to study the behaviour of the carbonyl carbon resonances in more detail.

Introduction

Recent advances in multidimensional NMR spectroscopy together with isotopic enrichment techniques have enabled essentially complete assignments of proton and heteronuclei (^{15}N and ^{13}C) resonances in proteins of a molecular mass up to 30 kDa (Grzesiek et al., 1992; Yamazaki et al., 1993; Fogh et al., 1995). The NOE-derived distance constraints together with homo- and heteronuclear coupling constants have permitted the first detailed studies of the solution structures of such proteins. For a complete description, knowledge of the dynamic properties of proteins also seems necessary. These parameters can be obtained by NMR relaxation experiments for certain time windows. In the past few years a significant number of studies have appeared in the literature describing the backbone dynamics of a wide variety of uniformly ^{15}N-labelled proteins based on measurements of ^{15}N T_1 and T_2 relaxation times as well as the steady-state ^1H-^{15}N NOE values (Kay et al., 1989; Clore et al., 1990a,b; Barbato et al., 1992; Fushman et al., 1994). The analysis of the relaxation data using a suitable model of motion provides dynamical parameters of the motion of the N-H bond. Since a typical property of protein structures is the planarity of the peptide plane, the motion of the N-H bond should be highly correlated with the motion of the C=O bond. Therefore, it should also be possible to study the dynamics of the peptide plane using carbonyl relaxation times. This way has, in contrast to ^{15}N relaxation time measurements, three major advantages: no artefacts arise due to H^N exchange with water protons; furthermore, proline residues are detectable and, as shown below, the relation between the measured relaxation times and the spectral density function is relatively simple.

*To whom correspondence should be addressed.

Supplementary Material: Three tables containing the T_1 and T_2 relaxation times of the carbonyl carbons of ribonuclease T1 at 500, 600 and 800 MHz, the results from the first level approach, and the results from the second level approach are available from the authors on request.

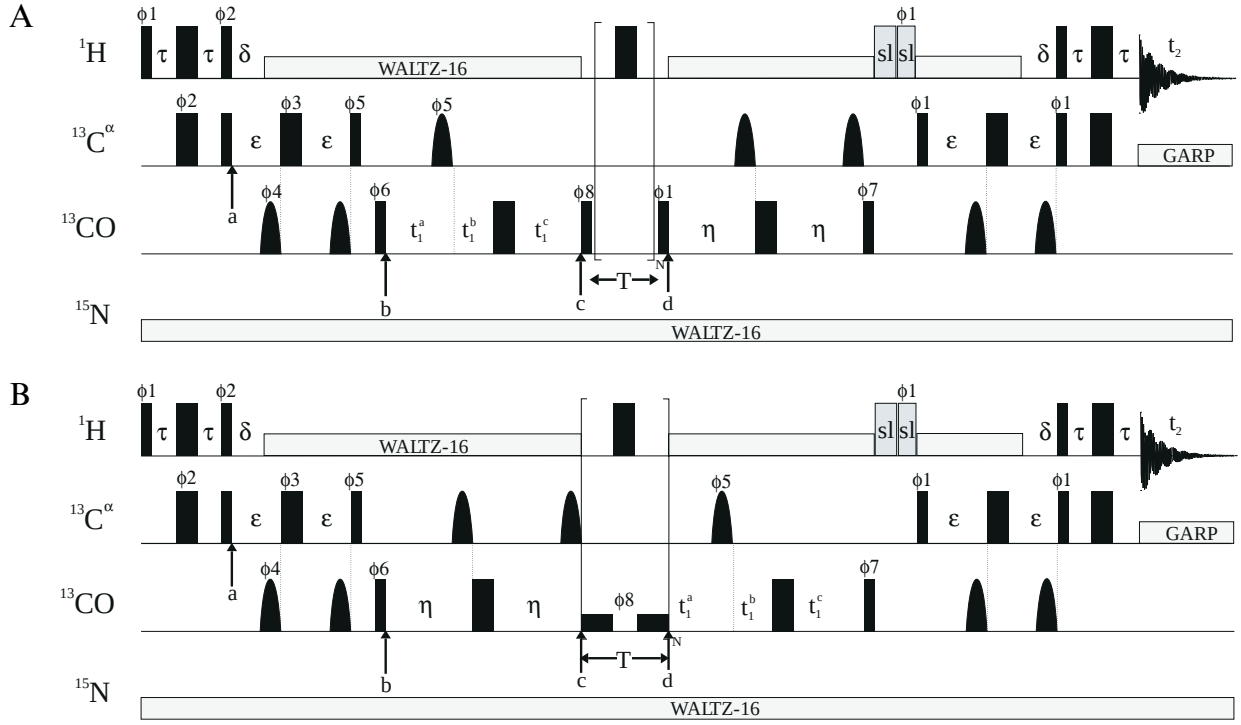

Fig. 1. Pulse sequences used for the measurement of $^{13}C'$ T_1 (A) and T_2 (B) values with ^1H detection. Narrow and broad rectangles indicate pulses with flip angles of 90° and 180°, respectively. Pulses for which the phase is not indicated were applied along the x-axis. Spin-lock (sl) ^1H pulses with durations of 2 ms and 1 ms are applied along the x- and y-axis, respectively, to suppress the residual water signal and magnetization originating from protons not directly coupled to ^{13}C. The carrier frequency in the ^{13}C channel was switched between the 90° ^{13}C pulses Φ5 and Φ6 from the $^{13}C^{\alpha}$ region (56 ppm) to the carbonyl carbon region (177 ppm) and back between Φ7 and Φ1. The power of the 90° and 180° $^{13}C^{\alpha}$ pulses was adjusted such that they did not excite the $^{13}C'$ nuclei ($\tau^{90}=\sqrt{15}/(4\Delta\Omega)$ and $\tau^{180}=\sqrt{3}/(2\Delta\Omega)$ with $\Delta\Omega=15.2$ kHz (500 MHz), 18.3 kHz (600 MHz) and 24.3 kHz (800 MHz)). The off-resonance $^{13}C^{\alpha}$ pulses had a square shape and their rf field strength was adjusted to $\gamma B_1=\Delta\Omega/\sqrt{3}$. Sinc-shaped phase-modulated off-resonance DANTE pulses with an rf field strength of 2500 Hz (500 MHz, 600 MHz) and 3300 Hz (800 MHz) were used to excite the carbonyl carbons downfield from the ^{13}C carrier. The ^{13}C pulses for the carbonyl absorption region were tuned to a value of $\gamma B_1=\Delta\Omega/\sqrt{15}$ such that the $^{13}C^{\alpha}$ carbons were not affected. ^1H and ^{15}N decoupling was accomplished using WALTZ-16 with a field of 3200 Hz and a 900 Hz rf field, respectively. $^{13}C^{\alpha}$ decoupling during acquisition was achieved using the GARP modulation with a field strength of 3.2 kHz. Delay durations were: $\tau=1.7$ ms, $\delta=3.4$ ms, $\varepsilon=3.6$ ms, $\eta=4.5$ ms, $t_1^a=4.5$ ms, $t_1^b=4$ μs, $t_1^c=4.5$ ms. The phase cycling used was as follows: Φ1 = y; Φ2 = x,–x; Φ4 = 8(x),8(–x); Φ5 = 4(x),4(–x); Φ6 = 2(x),2(–x); for a, Φ3 = 16(x),16(y),16(–x),16(–y); Φ7 = x,–x; Φ8 = 8(y+40°),8(–y+40°) (Bloch–Siegert phase error compensation); acq. = P,–P,–P,P,–P,P,P,–P with P = (x,x,–x,–x); for b, Φ3 = 8(x),8(y),8(–x),8(–y); Φ7 = (x+40°,–x+40°); Φ8 = 4(x),4(–x); acq. = P,–P,–P,P with P = (x,x,–x,–x). Quadrature detection is achieved by TPPI of Φ6 for scheme A and Φ7 for scheme B.

The measurement and interpretation of $^{13}C'$ relaxation times in highly enriched, uniformly $^{13}C/^{15}N$-labelled proteins are not as straightforward as for ^{15}N relaxation times (Yamazaki et al., 1994; Engelke and Rüterjans, 1995). In order to use the advantage of sensitivity enhancement associated with proton-detected experiments, the magnetization has to be transferred from the $^1H^{\alpha}$ to the carbonyl carbon and back in an HCACO-type experiment (Kay et al., 1990; Powers et al., 1991). During the transverse relaxation period, the presence of the scalar coupling between $^{13}C^{\alpha}$ and $^{13}C'$ may induce relaxation of the second kind, unless precaution is taken. In addition, the type of relaxation mechanism has to be considered. The nuclear spin relaxation of the amide nitrogen in a ^{15}N-labelled protein stems mainly from the dipole–dipole interaction between the amide nitrogen and its directly bound hydrogen. A minor part of the relaxation is caused by the ^{15}N chemical shift anisotropy (CSA). In this case the amide ^{15}N-^1H pair is an isolated AX-spin system. In a completely $^{13}C/^{15}N$-labelled protein the $^{13}C'$ nucleus is surrounded by several other nuclei with a nuclear spin and therefore CSA and various dipole–dipole interactions contribute to its relaxation. This environment implies that, for a realistic interpretation of the carbonyl carbon relaxation times, a detailed analysis of the relative contributions of all possible relaxation mechanisms is necessary.

For the analysis the relaxation rates of a particular backbone carbonyl nucleus are related to its spectral density function. The most common approach to extract information about dynamics from relaxation parameters is using the model-free spectral density function described by Lipari and Szabo (1982). In our study we also apply this procedure as a 'first level approach'. While this method is very powerful for extracting dynamical parameters from ^{15}N relaxation data, its applicability to carbonyl carbon relaxation data is less certain. Therefore, we have chosen to obtain further proof for this analysis by mapping the spectral density function ('second level approach')

(Peng and Wagner, 1992) using relaxation rates from three different spectrometer frequencies.

Materials and Methods

NMR spectrometers and sample preparation

The NMR experiments were performed on Bruker DMX500, DMX600 and DMX800 spectrometers, equipped with triple-resonance $^{15}N/^{13}C/^{1}H$ probe heads, operating at 308 K. Uniformly $^{15}N/^{13}C$-enriched ribonuclease T1 (RNase T1) was dissolved in 99.99% D_2O to a final concentration of 2.2 mM, the pH being adjusted to 5.5.

Pulse sequences used to determine carbonyl relaxation times

For studying the backbone dynamics of proteins with $^{13}C^{\alpha}$, $^{13}C'$ and ^{15}N relaxation times, the use of only one sample of a uniformly $^{13}C/^{15}N$-enriched protein dissolved in H_2O would be reasonable. For uniformly enriched samples the application of pulse sequences using an HNCO type instead of the HCACO type of magnetization transfer would be preferable (Dayie and Wagner, 1995; Zeng et al., 1996). Nevertheless, we used the latter one, since the $^{13}C^{\alpha}$ relaxation times were determined with a sample in D_2O separately, the contribution of the dipole–dipole interaction between $^{13}C'$ and H^N to the relaxation of the carbonyl carbon does not have to be considered (see below), and furthermore we wanted to extend our investigations to the carbonyl and carboxyl resonances of the side chains of asparagine, glutamine, aspartic and glutamic acid residues. Figures 1A and B illustrate the pulse schemes used for recording the $^{13}C'$ T_1 (A) and T_2 (B) relaxation times in more than 95% enriched, uniformly $^{13}C/^{15}N$-labelled RNase T1.

The experiments are based on magnetization transfer in an HCACO manner, yielding two-dimensional spectra with a carbonyl carbon dimension in F1 and a $^{1}H^{\alpha}$ dimension in F2. The details of this type of correlation have been

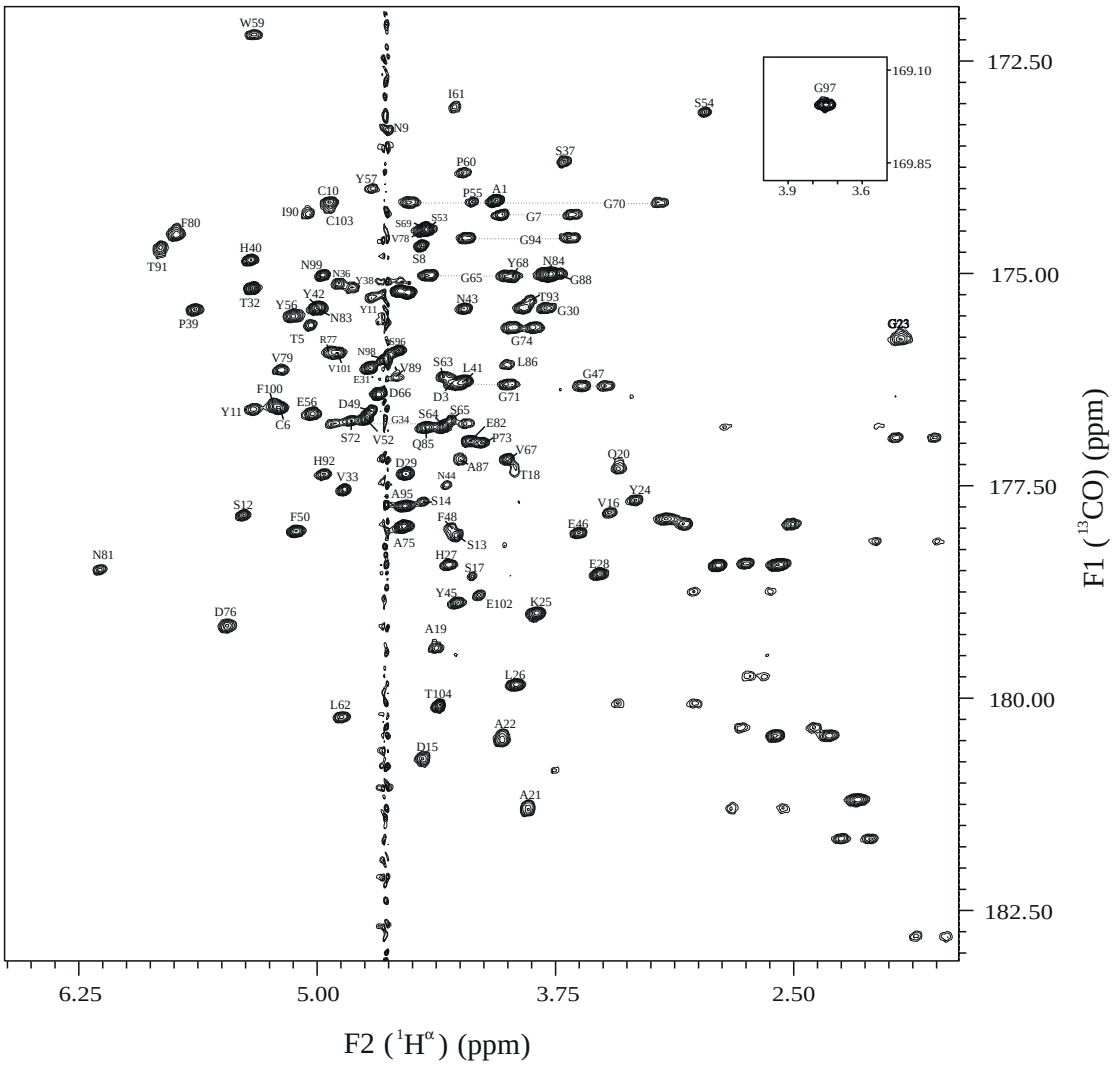

Fig. 2. First $^{1}H^{\alpha}$-$^{13}C'$ correlation spectrum from a series for T_1 relaxation time measurements at 600 MHz. Cross-peak assignments are indicated with the one-letter amino acid code and the residue number. The horizontal lines indicate the correlations between the glycine protons.

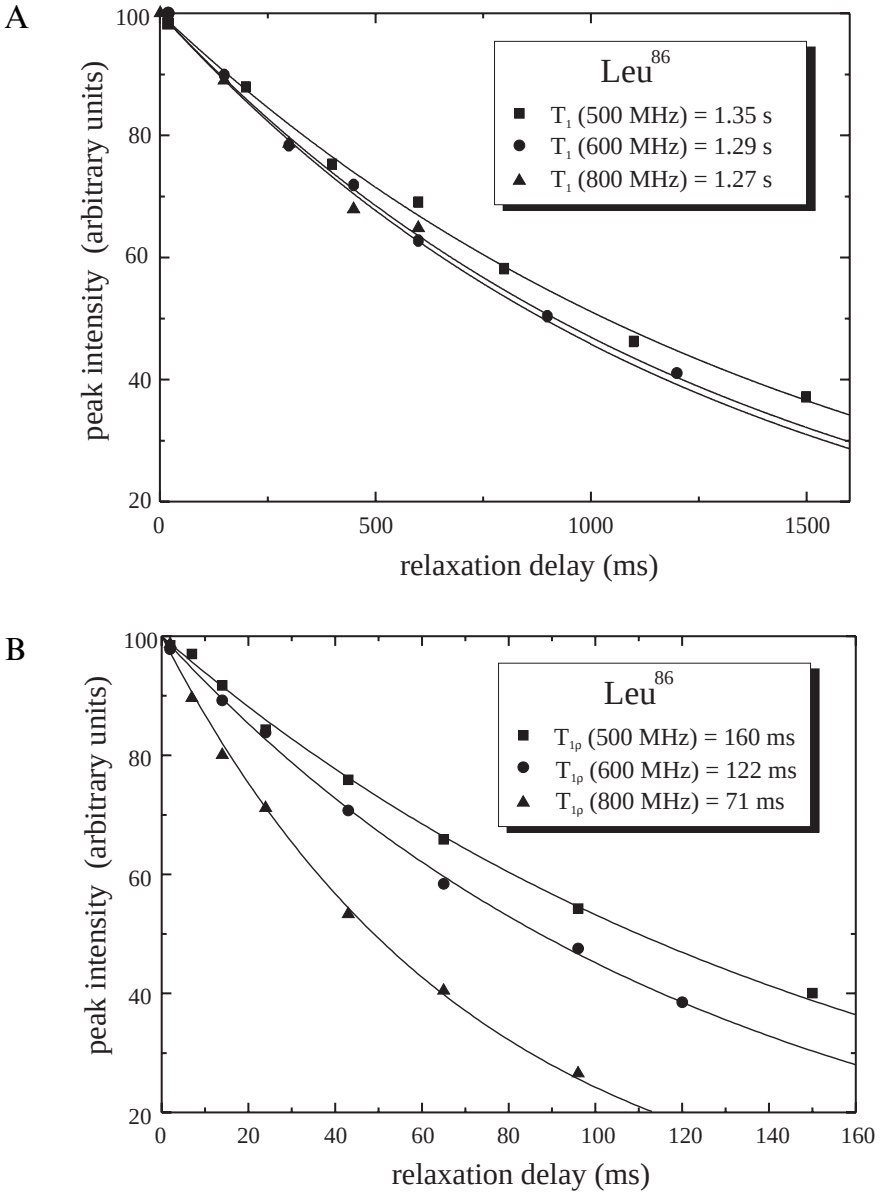

Fig. 3. Experimental and calculated intensity decay curves for the longitudinal (A) and transverse (B) relaxation of $^{13}C'$ of Leu^{86} at 500, 600 and 800 MHz.

reported by Grzesiek and Bax (1993), and only a brief description of the modifications with respect to the original pulse sequence is given, which is necessary for the determination of carbonyl relaxation times. The initial INEPT sequence transfers longitudinal $^{1}H^{\alpha}$ magnetization into antiphase $^{13}C^{\alpha}$ magnetization at a (Fig. 1A). During the delay 2ε, antiphase magnetization of $^{13}C^{\alpha}$ with respect to the carbonyl is produced with simultaneous refocusing of $^{1}H^{\alpha}$-$^{13}C^{\alpha}$ antiphase magnetization and synchronous proton decoupling. Simultaneous 90° pulses on $^{13}C^{\alpha}$ and $^{13}C'$ channels result in an INEPT-type transfer, with $^{13}C'$ magnetization now transverse and antiphase with respect to $^{13}C^{\alpha}$ (b in Fig. 1A). Subsequently, $^{13}C'$ magnetization evolves during the semi-constant-time t_1 delay ($t_1 = t_1^a + t_1^b - t_1^c$), with refocusing of antiphase magnetization occurring for a duration of $t_1^a - t_1^b + t_1^c = 1/2J_{C^{\alpha}C'}$, such that at c in the pulse sequence the signal is in phase. During the following period between c and d a specific pulse scheme is applied depending on whether the longitudinal relaxation times (Fig. 1A) or the transverse relaxation times (Fig. 1B) should be determined. In order to suppress cross-correlation between CSA and $^{13}C'$-$^{1}H^{\alpha}$ dipole–dipole relaxation, 180° ^{1}H pulses are applied during the relaxation delay (Boyd et al., 1990). Finally the magnetization is transferred back to $^{1}H^{\alpha}$ by two successive INEPT transfers for detection during t_2.

In order to obtain T_1 relaxation times, the inversion recovery scheme is used between c and d (Fig. 1A). Phase alternation of Φ10 is applied in order to store magnetization along the +z- and –z-axis such that the magnetization

may relax with $\exp(-t/T_1)$. In this way a less optimal delay between scans will only affect the sensitivity of the experiment without introducing systematic errors (Sklenář et al., 1987). Series of seven 2D spectra were recorded with T delays of 2, 150, 300, 450, 600, 900 and 1200 ms. The measuring time varied between 5 and 11 h for each spectrum, depending on the T delay.

For measuring the transverse relaxation times, we applied a spin-lock pulse ($T_{1\rho}$). For its rf field strength a value of 3000 Hz was used, providing a tip angle between 78° and 90° for all $^{13}C'$ resonances at 600 MHz. This results in a maximal difference of 5% between the $T_{1\rho}$ and T_2 values (Peng and Wagner, 1992). In order to ensure that in each increment at the beginning of the transverse relaxation period the carbonyl magnetization is on the +x- or −x-axis, the t_1 evolution period is placed behind the relaxation period. Series of seven or eight 2D spectra were acquired in approximately 5 h with T delays of 2.4, 7.2, 14.4, 24, 43.2, 64.8, 96 and 120 ms.

Data evaluation

The data sets were recorded as 180×1024 (500 MHz), 220×1024 (600 MHz) and 288×1024 (800 MHz) real matrices with 64 scans for each t_1 value and a spectral width of 11 ppm in F1 and 5 ppm in F2. Apodization, zero-filling and Fourier transformation led to a digital resolution of 2.2 Hz/point in F1 and 1.9 Hz/point in the F2 dimension. The spectra were processed and analysed on a Silicon Graphics workstation using the UXNMR and AURELIA programs (Bruker Analytische Messtechnik GmbH, Karlsruhe, Germany).

Figure 2 shows the first spectrum out of the series of 2D spectra for measuring T_1. For the assignment of the $^1H^\alpha$ and the $^{13}C'$ resonances in RNase T1, standard triple-resonance experiments carried out in H_2O and D_2O were used (Pfeiffer et al., 1996). In the present work, 84 (500 MHz) and 94 (600 MHz, 800 MHz) of the 104 cross peaks were sufficiently well resolved such that they could be considered during the data analysis.

For the evaluation of relaxation times, the intensities of corresponding resonances in this series of 2D spectra were fitted to a single exponential, depending on the relaxation delay. The fit was performed using a least-squares minimization procedure based on a downhill-simplex algorithm (Press et al., 1988) and the margin of errors was determined by a Monte Carlo approach using the method of simulated experimental data (Kamath and Shriver, 1989). Typical decay curves as well as their best fits are shown in Fig. 3.

Relaxation properties of the carbonyl carbon resonance

In a uniformly $^{13}C/^{15}N$-labelled protein, various different spins are located in the vicinity of the $^{13}C'$ spin such that the analysis of its relaxation behaviour is more complicated than for the backbone ^{15}N. At high magnetic field strength the relaxation of the protein peptide carbonyl carbon is dominated by the chemical shift anisotropy (CSA) relaxation, although the contributions of the various dipole–dipole interactions between the $^{13}C'$ spin and the adjacent spins may not be neglected a priori. The relevant expressions for the CSA relaxation are (Abragam, 1961; Goldman, 1984):

$$(1/T_1)_{CSA} = \rho^1_{CSA} = d^2_{CSA}\omega_C^2 J_{C'}(\omega_C) \quad (1a)$$

$$(1/T_2)_{CSA} = \rho^2_{CSA} = (d^2_{CSA}\omega_C^2/6)[4J_{C'}(0) + 3J_{C'}(\omega_C)] \quad (1b)$$

where

$$d^2_{CSA} = (1/3)\Delta\delta^2[1 + \xi^2_{CSA}/3] \quad (2)$$

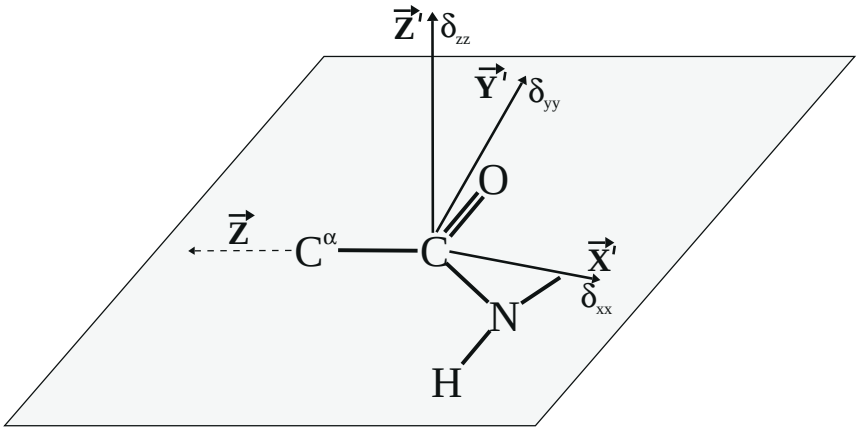

Fig. 4. Orientation of the peptide carbonyl ^{13}C chemical shift tensor. The carbonyl group and the amide nitrogen are in approximately the same plane. The $\vec{X}'$ and $\vec{Y}'$ principal axes of the CSA tensor have been located in this plane and form angles of 77° and 13°, respectively, with the CO bond. The direction of $\vec{Z}'$ is located perpendicular to this plane. The values of the angle θ between the $^{13}C'$-$^{13}C^\alpha$ bond ($\vec{Z}$-axes) and the $\vec{X}'$, $\vec{Y}'$ and $\vec{Z}'$ axes are given by: $\theta'_{XZ} = 197°$, $\theta'_{YZ} = 107°$ and $\theta'_{ZZ} = 90°$. The values of the principal axes of the CSA tensor used in this calculation were: $\delta_{xx} = -115.6$ ppm, $\delta_{yy} = -48.6$ ppm and $\delta_{zz} = +40.6$ ppm (Stark et al., 1983).

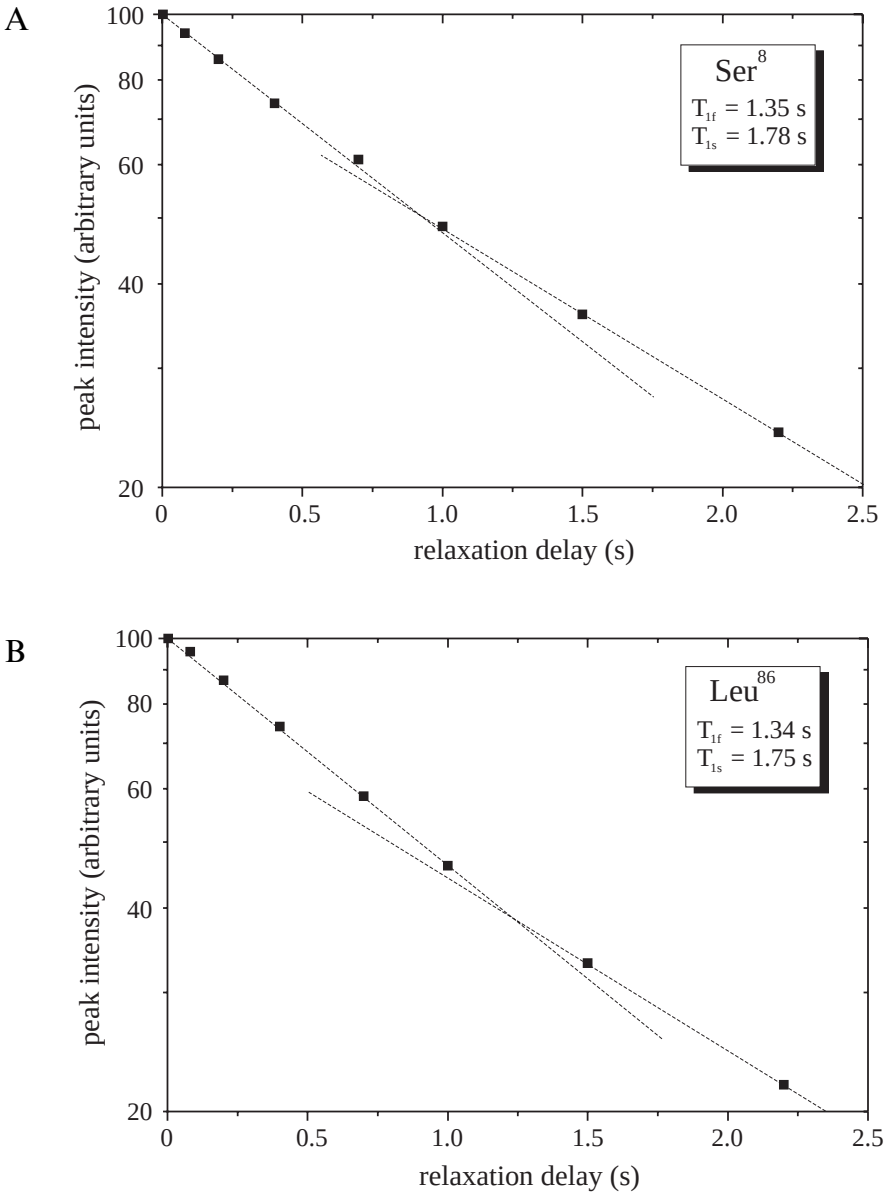

Fig. 5. Experimental and calculated intensity decay curves for the longitudinal relaxation of the carbonyl carbon of Ser[8] and Leu[86] of ribonuclease T1. The experimental data were fitted to a biexponential function of the form $I = A_1 \exp(-T/T_{1f}) + A_2 \exp(-T/T_{1s})$, where T is the relaxation delay. In order to show the biexponential decay more explicitly, the ordinate scale is logarithmic.

with $\Delta\delta = \delta_{zz} - (1/2)(\delta_{xx}+\delta_{yy})$, $\xi_{CSA} = (\delta_{xx}-\delta_{yy})/(\delta_{zz}-\delta_0)$ and $\delta_0 = (1/3)(\delta_{xx}+\delta_{yy}+\delta_{zz})$. Note that, in contrast to the ^{15}N chemical shielding tensor, the assumption of an axially symmetrical shift tensor for the carbonyl carbon cannot be used (Stark et al., 1983). In Eqs. 1 and 2, δ_{ii} are the diagonal elements of the chemical shift tensor defined in Fig. 4, ω_C is the resonance frequency of the carbon nucleus and $J(\omega)$ is the corresponding spectral density function. Since experimental values for the components of the chemical shift tensor of protein carbonyl carbons in solution are not yet available, we had to take advantage of previous results from solid-state investigations of smaller peptides. Stark et al. (1983) investigated the carbonyl shielding tensor in a single crystal of the dipeptide [1-^{13}C]glycyl[^{15}N]glycine.

TABLE 1
DIPOLE–DIPOLE INTERACTION CONSTANT c^2_{AB} FOR THE INTERACTIONS BETWEEN THE ^{13}C' CARBON AND THE ADJACENT NUCLEI

Interacting nuclei	Distance r (Å)	c^2_{AB} (10^9 s^{-2})
C'-C^α	1.53	0.044
C'-C^β	2.51	0.002
C'-H^α	2.17	0.086
C'-N	1.32	0.017
C'-H^N [a]	2.03	0.129

The following values are assumed: $h = 6.626 \times 10^{-34}$ J s, $\mu_0 = 4\pi \times 10^{-7}$ T mA, $\gamma_H = 2.6752 \times 10^8$ s^{-1} T^{-1}, $\gamma_C = 6.728 \times 10^7$ s^{-1} T^{-1}, $\gamma_N = 2.709 \times 10^7$ s^{-1} T^{-1}.

[a] This dipole–dipole interaction only has to be considered for an H_2O sample.

They determined a value of 6.2×10^{-9} for d^2_{CSA}. Ye et al. (1993) measured the tensor components of the carbonyl carbon of polycrystalline powders of 20 amino acids by CP/MAS spectroscopy, and the d^2_{CSA} value for glycine calculated from these data was 4.9×10^{-9}. This difference of about 25% seems to be an indication that the value of d^2_{CSA} depends strongly on the sample and the experimental conditions. Therefore, it is open to question as to whether these values obtained from peptides in the solid state can be applied to carbonyl carbons of proteins in solution. Furthermore, it is not clear whether the same d^2_{CSA} value can be applied to all types of amino acids. Indeed, this is a critical point in the analysis. Nevertheless, in order to start with a first attempt in our analysis we decided to use a d^2_{CSA} value of 6.2×10^{-9} for all amino acid types.

The contribution of the various dipole–dipole interactions between the $^{13}C'$ spin and the adjacent spins will now be analysed in detail. In the case of random isotropic molecular reorientation, the following expressions for an individual ^{13}C carbonyl carbon in the absence of cross-relaxation (see below) may be written (Abragam, 1961; Bull, 1992):

$$\left(\frac{1}{T_1}\right)_{DD} = \rho^1_{C'X} = \sum_{X=1}^{N} c^2_{C'X}\left[J_{C'X}(\omega_X - \omega_C) + 3J_{C'X}(\omega_C) + 6J_{C'X}(\omega_X + \omega_C)\right] \quad (3a)$$

$$\left(\frac{1}{T_2}\right)_{DD} = \rho^2_{C'X} = \sum_{X=1}^{N} \frac{c^2_{C'X}}{2}\left[4J_{C'X}(0) + J_{C'X}(\omega_X - \omega_C) + 3J_{C'X}(\omega_C) + 6J_{C'X}(\omega_X) + 6J_{C'X}(\omega_X + \omega_C)\right] \quad (3b)$$

where

$$c^2_{C'X} = \frac{\gamma^2_C \gamma^2_X}{4\langle r^3_{C'X}\rangle^2}\left(\frac{h}{2\pi}\right)^2\left(\frac{\mu_0}{4\pi}\right)^2 \quad (4)$$

N is the number of spins X (X = ^1H, ^{13}C, ^{15}N) responsible for dipole–dipole relaxation, $J_{C'X}(\omega)$ characterizes the motion of the two interacting spins, h is Planck's constant, $\langle r_{C'X}\rangle$ is the distance between the carbonyl carbon and the X nucleus responsible for relaxation, and γ_C and γ_X are the gyromagnetic ratios of the carbon spin and the X spin, respectively. In general, all spins in a protein

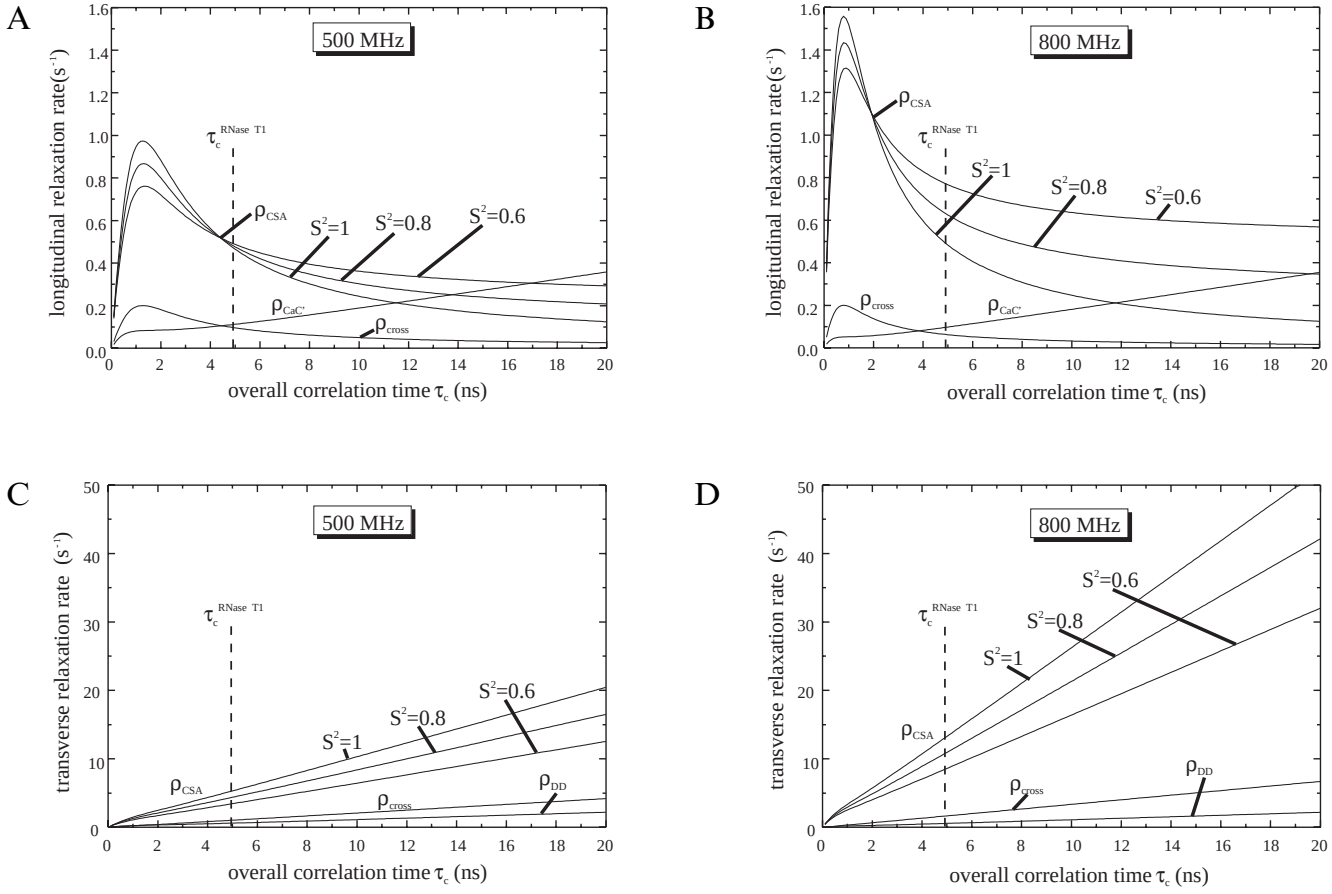

Fig. 6. Theoretical longitudinal (A, B) and transverse (C, D) relaxation rates of $^{13}C'$ as a function of the isotropic correlation time τ_c and the spectrometer frequencies. Values for the CSA relaxation rate ρ_{CSA}, the dipole–dipole relaxation rate $\rho_{C'C^\alpha}$, ρ_{DD} and the relaxation due to the cross-correlation ρ_{cross} are indicated. In order to describe the motion of the CSA tensor, the spectral density function of Lipari and Szabo with an internal correlation time τ_i of 350 ps was used in this calculation.

contribute to the relaxation of an individual ^{13}C carbonyl carbon, but the contribution of most of these spins can be neglected because of their large distance. For the few spins close enough to the carbonyl carbon, the values of $c^2_{C'X}$ are listed in Table 1.

For the relaxation time T_1, only the homonuclear $^{13}C^{\alpha}$-$^{13}C'$ interaction which is proportional to J(0) has to be considered. In proteins, J(0) is much larger than $J(\omega_C)$ and consequently the product $c^2_{C'C\alpha}J(0)$ becomes comparable to the product $d^2_{CSA}\omega^2_C J(\omega_C)$. Since the other dipole–dipole interactions between the carbonyl carbon and the ^{15}N, $^{1}H^{\alpha}$ and $^{13}C^{\beta}$ nuclei are heteronuclear and thus proportional to $J(\omega_C)$, the relation of their relaxation contributions to the contribution due to CSA relaxation is given with a good approximation by $3\sum c^2_{AB}/d^2\omega^2$. When the protein is dissolved in D_2O this relation amounts to 8% for 500 MHz, 6% for 600 MHz and 3% for 800 MHz, while for an H_2O protein sample these contributions are more than twice as large. Since a D_2O protein sample is used in this study, it seems reasonable to neglect these contributions, particularly for high magnetic field strengths. Since the contribution of the cross-relaxation between the $^{13}C'$ and the $^{13}C^{\alpha}$ leads to a cross peak at the $^{1}H^{\alpha}$-$^{13}C^{\alpha}$ frequency (Engelke and Rüterjans, 1995), it does not influence the intensity of the $^{1}H^{\alpha}$-$^{13}C'$ cross-peak intensity on which the determination of the T_1 relaxation time is based.

In the case of T_2 relaxation times, the CSA and all dipole–dipole interactions are proportional to J(0) and hence we have to consider the CSA relaxation and, for a D_2O protein sample, the contributions of the $^{13}C'$-$^{13}C^{\alpha}$ and $^{13}C'$-$^{1}H^{\alpha}$ interactions. The contribution of the dipolar interaction between the carbonyl carbon and the ^{15}N and $^{13}C^{\beta}$ nuclei is in the range of 1–2% and therefore negligible.

In addition, a third relaxation mechanism has to be discussed. It originates from the cross-correlation between CSA and dipolar $^{13}C'$-$^{13}C^{\alpha}$ relaxation. This contribution accelerates or reduces the relaxation of the carbonyl carbon, depending on whether the adjacent $^{13}C^{\alpha}$ spin is up or down (Goldman, 1984; Bull, 1992), according to:

$$(1/T_1)_{cross} = \rho^1_{cross} = \pm 2c_{C'C\alpha}\omega_C \alpha J_{C'C\alpha}(\omega_C) \qquad (5a)$$

$$(1/T_2)_{cross} = \rho^2_{cross} = \pm c_{C'C\alpha}\omega_C \alpha[(4/3)J_{C'C\alpha}(0) + J_{C'C\alpha}(\omega_C)] \qquad (5b)$$

with $\alpha = (1/2)[\delta_{xx}(3\cos^2\theta_{X'Z} - 1) + \delta_{yy}(3\cos^2\theta_{Y'Z} - 1) + \delta_{zz} \times (3\cos^2\theta_{Z'Z} - 1)]$. The values and the meaning of δ and θ are demonstrated in Fig. 4. The decay of the longitudinal and transverse magnetization is biexponential and the ratio of these two relaxation rates amounts to approximately 1.4 (600 MHz, $\tau_c = 4.9$ ns). Clearly, this effect can result in higher values of the measured relaxation rates if not properly accounted for in the interpretation of the relaxation data or if not adequately suppressed. In order to verify this relaxation contribution experimentally, we recorded a series of T_1 with additional delays of 1.5 and 2.2 s for T. As an example, the biexponential decay of T_1 as well as their best fits for Ser[8] and Leu[86] are shown in Fig. 5. The relation of 1.32 and 1.30 between the two relaxation rates agrees quite well with the theoretical considerations.

In the case of ^{15}N relaxation time measurements, this relaxation mechanism is suppressed by applying 180° proton pulses during the relaxation period (Boyd et al., 1990; Kay et al., 1992). We tried to use this technique as well by applying G3 pulses to the $^{13}C^{\alpha}$ carbon, but the errors in the exponential decays increased. This may be due to an imperfect selectivity of the G3 pulses and the fact that the number of such pulses depends on the length of the relaxation period T. An additional problem arises from Bloch–Siegert shifts in the case of measuring $T_{1\rho}$. Therefore, we decided to evaluate the relaxation rates from the initial T delays and take this relaxation mechanism into account while calculating the microdynamical parameters. Since the dipolar interaction constant $c^2_{C'N}$ is very small, the contribution of the cross correlation between the CSA relaxation of the carbonyl carbon and the dipolar $^{13}C'$-^{15}N interaction can be neglected.

Certainly, also the contribution of conformational exchange R_{ex} has to be taken into account for some residues, so that the total relaxation rates are given by:

$$\frac{1}{T_1} = \underbrace{d^2_{CSA}\omega^2_C\, J_{C'}(\omega_C)}_{\rho^1_{CSA}} + \underbrace{2c_{C'C^{\alpha}}\omega_C \alpha\, J_{C'C^{\alpha}}(\omega_C)}_{\rho^1_{cross}} + \underbrace{c_{C'C^{\alpha}}\left[J_{C'C^{\alpha}}(0) + 3J_{C'C^{\alpha}}(\omega_C) + 6J_{C'C^{\alpha}}(2\omega_C)\right]}_{\rho^1_{C'C^{\alpha}}} \qquad (6a)$$

$$\frac{1}{T_2} = \underbrace{\frac{d^2_{CSA}\omega^2_C}{6}\left[4J_{C'}(0) + 3J_{C'}(\omega_C)\right]}_{\rho^2_{CSA}} + \underbrace{c_{C'C^{\alpha}}\omega_C \alpha\left[\frac{4}{3}J_{C'C^{\alpha}}(0) + J_{C'C^{\alpha}}(\omega_C)\right]}_{\rho^2_{cross}} + \underbrace{\rho^2_{C'C^{\alpha}} + \rho^2_{C'H^{\alpha}}}_{\rho^2_{DD}} + R_{ex} \qquad (6b)$$

Figure 6 shows the contribution of ρ_{CSA}, $\rho_{C'C\alpha}$, ρ_{DD} and ρ_{cross} to the longitudinal and transverse relaxation of the carbonyl carbon. For the longitudinal relaxation time, it is obvious that a simplification of Eq. 6a by omitting ρ_{CSA}, $\rho_{C'C\alpha}$ or ρ_{cross} is not possible, because these contributions are all of comparable order in the range between 1 and 20 ns. Their relative contributions depend on τ_c: for molecules with short correlation times the CSA relaxation mechanism dominates, while for proteins with longer rotational correlation times the contribution of $\rho_{C'C\alpha}$ to T_1

increases steadily. In the case of the transverse relaxation time, the contributions of ρ_{DD} and ρ_{cross} are certainly smaller, but nevertheless they have to be considered.

Analysis of the relaxation times

In order to analyse the relaxation rates, we applied two different approaches. At the first level the formalism of Lipari and Szabo (1982) is used, and an analytical expression for the microdynamical parameters has been derived. For this approach only two measured relaxation rates are necessary and this procedure is applicable when the overall correlation time of the molecule is known. The second level is more sophisticated. We mapped the spectral density function using six relaxation rates measured at three different spectrometer frequencies. Furthermore, a value for the conformational exchange can be extracted for each residue.

First level approach

In order to derive dynamical parameters from the measured relaxation times, it is necessary to choose a suitable model of motion that describes the motion of the carbonyl shielding tensor. In the present work this will be achieved by using the 'model-free approach' formalism introduced by Lipari and Szabo (1982), well known from the analysis of ^{15}N relaxation data. In this model $J(\omega_i)$ is expressed according to

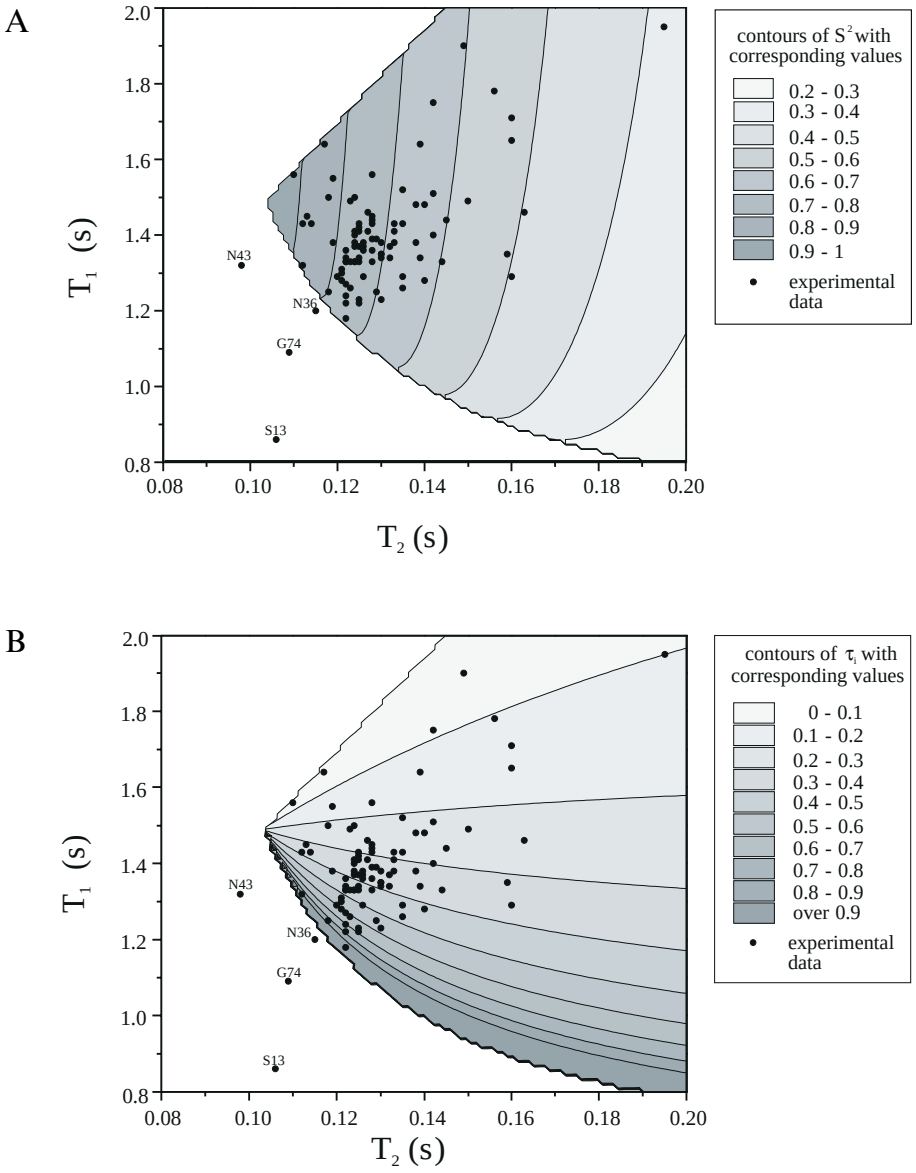

Fig. 7. Contour plots of the calculated areas of S^2 (A) and τ_i (B) in dependence of the longitudinal and transverse relaxation times at 600 MHz. In this calculation the overall correlation time τ_c was assumed to be 4.9 ns. For the anisotropy constant d^2_{CSA}, a value of 6.2×10^{-9} was derived from Stark et al. (1983). The experimental data obtained for the residues of ribonuclease T1 are indicated with filled circles.

$$J(\omega) = \frac{2}{5}\left[\frac{S^2\tau_c}{1+(\omega\tau_c)^2} + \frac{(1-S^2)\tau_i}{1+(\omega\tau_i)^2}\right] \quad (7)$$

with $\tau_i^{-1} = \tau_c^{-1}+\tau_e^{-1}$, where τ_c is the isotropic tumbling time and τ_e is an effective internal correlation time. The order parameter S^2 characterizes the amplitude of local motion: S^2 is equal to 1 for a completely restricted internal motion, while S^2 is equal to 0 for an unrestricted internal reorientation. We would like to emphasize that this order parameter can be considered as an equilibrium average and contains no information about the time scale of internal dynamics. On the other hand, the effective correlation time τ_i that describes the rapid internal motion depends on both the microscopic diffusion or jump constant and the spatial nature of the motion. All calculations were performed assuming isotropic overall tumbling of the protein, which may be inferred from the ratio of the principal components of the inertia tensor of RNase T1 as calculated to be 1:1.14:1.27 from X-ray crystallographic data (Martinez-Oyanedel et al., 1991). Although this model is frequently used to describe the motion of the ^{15}N-^{1}H and $^{13}C^{\alpha}$-$^{1}H^{\alpha}$ bonds of the protein backbone, it must be emphasized that its application is limited to motions whose correlation function for the internal motion only decays following a single exponential (τ_i). This type of motion is typical for residues in α-helix or β-sheet secondary structures. For residues in loop regions it may be necessary to extend this model in some cases by additional time scales for the internal dynamic behaviour.

In order to limit the number of fitting parameters, it has been assumed that for all residues the flexibility of the link between the carbonyl carbon and the $^{13}C^{\alpha}$ and $^{1}H^{\alpha}$ can be described by an order parameter (S^2) of 0.8. Since the order parameter for most of the protein backbone nuclei ranges between 0.6 and 1, the margin of errors for the relaxation of the carbonyl carbons caused by this approximation amounts to approximately 5%. This assumption leads to a spectral density function of the form $J_{C'C^{\alpha}}(\omega) = J_{C'H^{\alpha}}(\omega) = (2/5)(0.8\tau_c)/(1+(\omega\tau_c)^2)$ such that the contribution of these dipole–dipole interactions is only a function of τ_c. One of the advantages of the carbonyl relaxation times in comparison to the ^{15}N relaxation concerns their analysis. No numerical procedure is necessary and the results can easily be represented because of the possibility to derive an analytical expression for the microdynamical parameters S^2 and τ_i. The details of this calculation are described in the Appendix, and only the solution is presented here. If the term for the conformational exchange R_{ex} is set to zero, then the expressions for the effective internal correlation times are given by

$$\tau_{i,1} = \tau_c \quad (8a)$$

$$\tau_{i,2} = -\frac{b}{2a} + \sqrt{\left(\frac{b}{2a}\right)^2 - \frac{c}{a}} \quad (8b)$$

$$\tau_{i,3} = -\frac{b}{2a} - \sqrt{\left(\frac{b}{2a}\right)^2 - \frac{c}{a}} \quad (8c)$$

and for the order parameter by

$$S^2 = 1 + b/(\tau_c - \tau_i) \quad (9)$$

with

$$a = \frac{5}{2}\frac{1+\omega_C^2\tau_c^2}{\omega_C^2 d_{CSA}^2 \tau_c}\left[\frac{1}{T_1} - \rho^1_{C'C^{\alpha}} - \rho^1_{cross}\right] - 1 \quad (10a)$$

$$b = \frac{15}{8\omega_C^2 d_{CSA}^2}\left[\left(\frac{2}{T_2} - 2\rho^2_{DD} - 2\rho^2_{cross}\right) - \left(\frac{1}{T_1} - \rho^1_{C'C^{\alpha}} - \rho^1_{cross}\right)\right] - \tau_c \quad (10b)$$

$$c = \frac{1}{\omega_C^2\tau_c}[a\tau_c - b] \quad (10c)$$

$\tau_{i,1}$ is not a reasonable solution since the effective internal correlation time should be smaller than τ_c. Therefore, $\tau_{i,2}$ and $\tau_{i,3}$ are the solutions of interest, assuming that they are real (the radicant in Eqs. 8b and 8c has to be positive) and that they lead to values larger than zero. From our experience in analysing the carbonyl relaxation data of RNase T1, one solution for τ_i is valid. If τ_i is known, the order parameter S^2 can be calculated using Eq. 9, whereas a meaningful value is only attained if b is smaller than zero (S^2 must be smaller than 1). Obviously, some conditions have to be fulfilled so that microdynamical parameters can be calculated. Figure 7 shows a contour plot of S^2 (A) and τ_i (B) as a function of T_1 and T_2. For a combination of T_1–T_2 values which leads to a point inside the hatched area (Fig. 7), a solution exists and the microdynamical parameters are directly derived. In case the combination of T_1–T_2 values is located outside the hatched area, no solution exists. For these cases it seems reasonable to assume that either the applied model of motion is not suitable or additional terms like conformational exchange terms have to be considered. Figure 7 also demonstrates that the order parameter S^2 is mainly determined by the transverse relaxation time (contour lines are parallel to the T_1 axis in A) while the T_1 values depend on the value of the internal correlation time τ_i (contour lines are parallel to the T_2 axis in B).

Second level approach

In order to obtain a more detailed insight into the dynamics of the protein backbone, a mapping of the spectral density function for each carbonyl carbon was tried. Therefore, we used Eqs. 6a and b and measured the T_1 and T_2 relaxation times at the three different spectrometer frequencies of 500, 600 and 800 MHz. This approach leads to the following equation system:

$$\begin{pmatrix} \frac{1}{T_1^{500}} \\ \frac{1}{T_2^{500}} \\ \frac{1}{T_1^{600}} \\ \frac{1}{T_2^{600}} \\ \frac{1}{T_1^{800}} \\ \frac{1}{T_2^{800}} \end{pmatrix} = d_{CSA}^2 \begin{pmatrix} 0 & \omega_{125}^2 & 0 & 0 \\ \frac{2}{3}\omega_{125}^2 & \frac{1}{2}\omega_{125}^2 & 0 & 0 \\ 0 & 0 & \omega_{150}^2 & 0 \\ \frac{2}{3}\omega_{150}^2 & 0 & \frac{1}{2}\omega_{150}^2 & 0 \\ 0 & 0 & 0 & \omega_{200}^2 \\ \frac{2}{3}\omega_{200}^2 & 0 & 0 & \frac{1}{2}\omega_{200}^2 \end{pmatrix} \begin{pmatrix} J(0) \\ J(\omega_{125}) \\ J(\omega_{150}) \\ J(\omega_{200}) \end{pmatrix} + \begin{pmatrix} \rho_{C'C^\alpha}^{1,500} + \rho_{cross}^{1,500} \\ \rho_{DD}^{2,500} + \rho_{cross}^{2,500} \\ \rho_{C'C^\alpha}^{1,600} + \rho_{cross}^{1,600} \\ \rho_{DD}^{2,600} + \rho_{cross}^{2,600} \\ \rho_{C'C^\alpha}^{1,800} + \rho_{cross}^{1,800} \\ \rho_{DD}^{2,800} + \rho_{cross}^{2,800} \end{pmatrix} + \begin{pmatrix} 0 \\ R_{ex} \\ 0 \\ R_{ex} \\ 0 \\ R_{ex} \end{pmatrix} \quad (11)$$

For the relaxation contributions of the dipole–dipole interactions and the cross-correlation mechanism, the same form of the spectral density function as in the first level approach is applied: $J_{C'C^\alpha}(\omega) = J_{C'H^\alpha}(\omega) = (2/5)(0.8\tau_c)/(1+(\omega\tau_c)^2)$. The five parameters $J(0)$, $J(\omega_{125})$, $J(\omega_{150})$, $J(\omega_{200})$ and R_{ex} can then be calculated by minimizing the following target function for each residue:

$$\Psi^2 = \sum_{i=500,600,800} \left[\left(\frac{T_{1,i}^{exp} - T_{1,i}^{calc}}{\sigma_{T_1}^i} \right)^2 + \left(\frac{T_{2,i}^{exp} - T_{2,i}^{calc}}{\sigma_{T_2}^i} \right)^2 \right] \quad (12)$$

Results and Discussion

The average values for the $^{13}C'$ longitudinal and transverse relaxation times derived from the 2D spectra at 500, 600 and 800 MHz are presented in Fig. 8. While the T_1 values vary only slightly with the strength of the magnetic field, the transverse relaxation rate is nearly proportional to ω^2. Indeed, this agrees well with the theoretical considerations since for high B_0 fields the CSA relaxation mechanism dominates and therefore a quadratic dependence is expected (Eq. 1b). This increase of the line width with the magnetic field strength should be considered in the choice of a spectrometer frequency for NMR investigations, which use the carbonyl carbon as a relayed nucleus or in an indirect evolution period. Since the resolution increases only linearly with the spectrometer frequency, the application of a reduced magnetic field strength may be more reasonable, in particular for larger proteins with short transverse carbonyl relaxation times. The nonzero value at $\omega = 0$ reflects the fact that a minor contribution to the relaxation of the carbonyl carbon stems from dipole–dipole interactions and from the conformational exchange term.

Results from the 'first level approach'

In order to evaluate the parameters for the internal dynamics, the overall correlation time τ_c has to be determined. Since only two relaxation rates for each B_0 field are available, the value of τ_c must be obtained from other investigations. Recently we measured $^{13}C^\alpha$ relaxation times

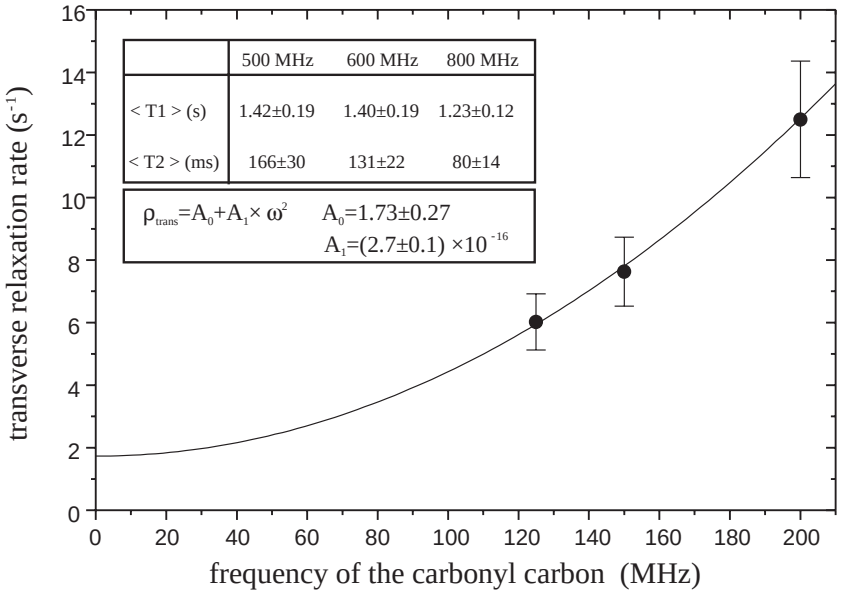

Fig. 8. Averages of relaxation rates depending on the static magnetic field strength. The calculated curve was obtained by fitting ρ_{trans} to the transverse relaxation rates using a simplex algorithm. The error of A_0 and A_1 was determined by a Monte Carlo simulation.

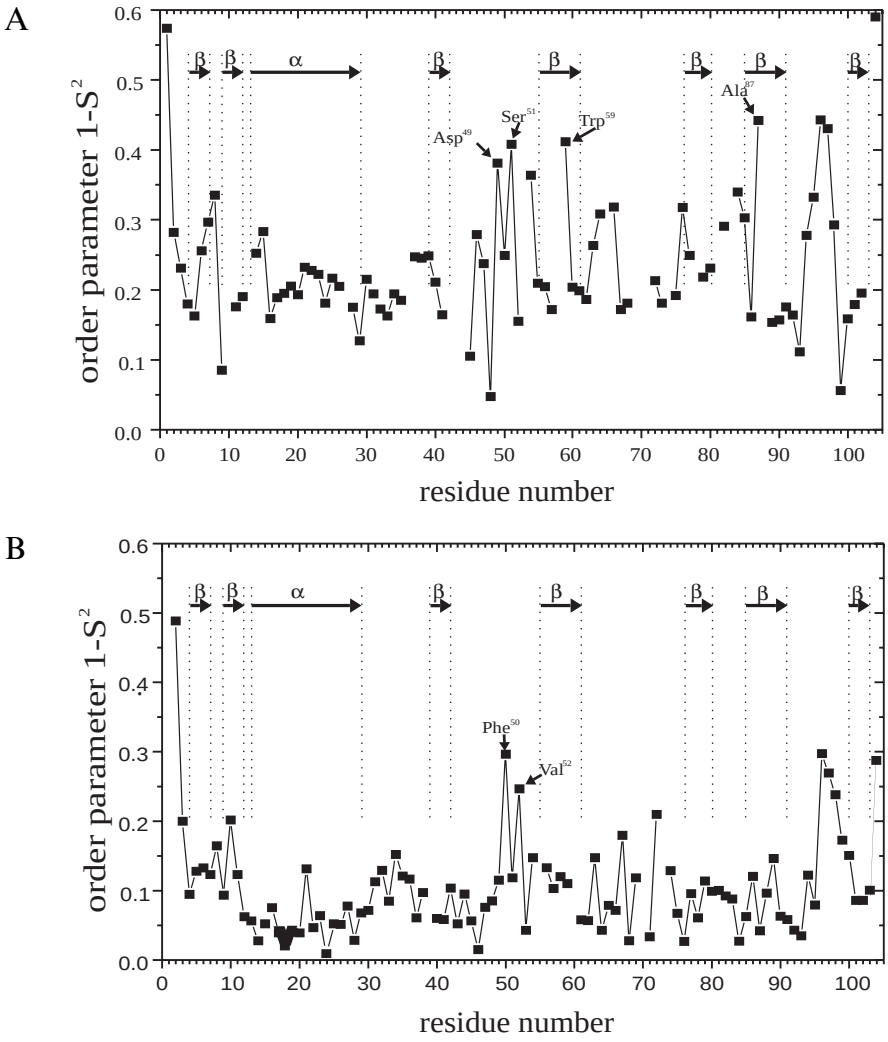

Fig. 9. Values of $1–S^2$ for the backbone carbonyl carbons (A) and amide nitrogens (B) of ribonuclease T1 plotted versus the amino acid sequence (Fushman et al., 1994; C. Ludwig, J. Engelke and H. Rüterjans, in preparation). The secondary structure elements are indicated with arrows.

of the same sample, and from this study we obtained a value of $\tau_c = 4.9 \pm 0.3$ ns. Although the viscosity of a D_2O sample should be about 20% larger than that of an H_2O sample, this value agrees well with the results from ^{15}N relaxation time measurements determined previously with an H_2O sample (Fushman et al., 1994). This agreement in τ_c might be caused by the lower protein concentration in the D_2O sample compensating the higher viscosity of the D_2O. Using this value of τ_c, the order parameter and the internal correlation time can be calculated using Eqs. 8 and 9. The corresponding contour plots are shown in Fig. 7.

In Fig. 9 the order parameters obtained from $^{13}C'$ and ^{15}N relaxation time measurements are plotted for the amino acid sequence of ribonuclease T1. In order to allow a direct comparison with other mobility parameters, $(1–S^2)$, being the deviation of S^2 from its complete restriction-limit value and therefore increasing with an increase in the amplitude of local motion, was chosen. From Fig. 9, differences in the internal mobility are obvious between the regions of regular secondary structure and the disordered structural elements. Small and homogeneous amplitudes of local motion were obtained for the residues belonging to the peripheral α-helix (residues 13–29), indicating a highly restricted local mobility of this part of the protein backbone. For the residues belonging to the strands of the central antiparallel β-sheet (residues 40–42, 56–61, 75–81, 86–92 and 100–103) of RNase T1, a restricted mobility for most of the residues was also observed. However, the order parameter $(1–S^2)$ of some residues in the β-sheet deviates considerably from that of their neighbours. This is, in particular, the case for Trp^{59} and Ala^{87}, for which long T_2 relaxation times were determined (160 and 163 ms, respectively) resulting in order parameters that are larger by a value of 0.2 than the values for the adjacent residues. Figure 10 depicts the neighbourhood of these residues. In both cases the dipole field of an aromatic ring system is close to the carbonyl

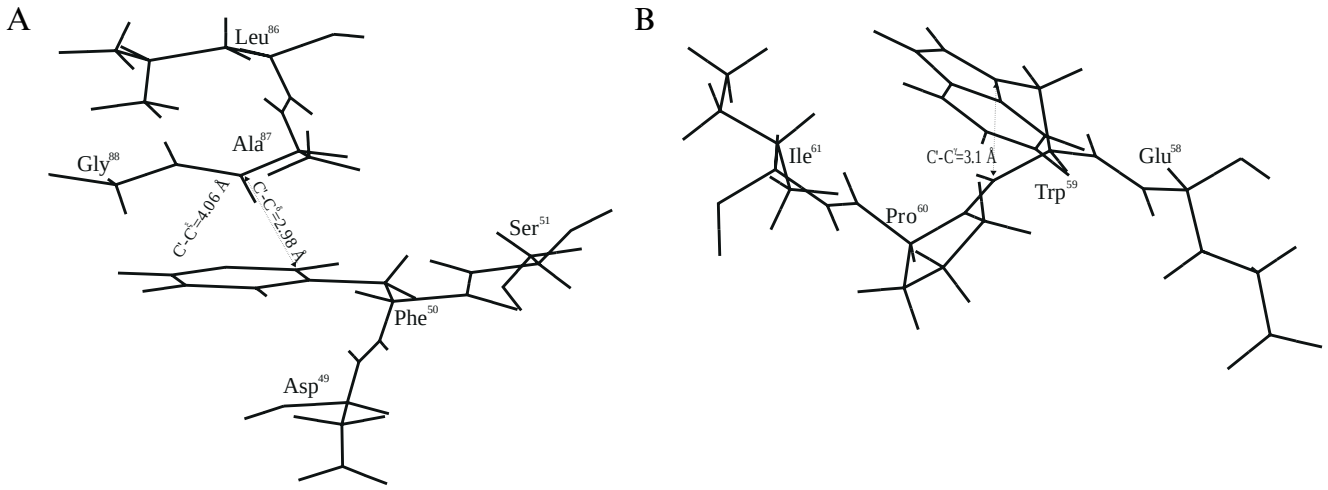

Fig. 10. The structural neighbourhood of Ala^{87} (A) and Trp^{59} (B) of ribonuclease T1. Details were obtained from the solution structure of ribonuclease T1 determined by NMR spectroscopy (S. Pfeiffer, J. Engelke and H. Rüterjans, in preparation).

carbon. Therefore, it seems reasonable to assume that this effect may influence the component of the CSA tensor that is perpendicular to the peptide plane. Since the relaxation rates are proportional to the product $d^2_{CSA}S^2$, a decrease of only 20 ppm of δ_{zz}, which changes the value of the anisotropy constant d^2_{CSA} by 25% (4.6×10^{-9}), would explain the observed change in the order parameters. As mentioned before, at this point the uncertainty of the

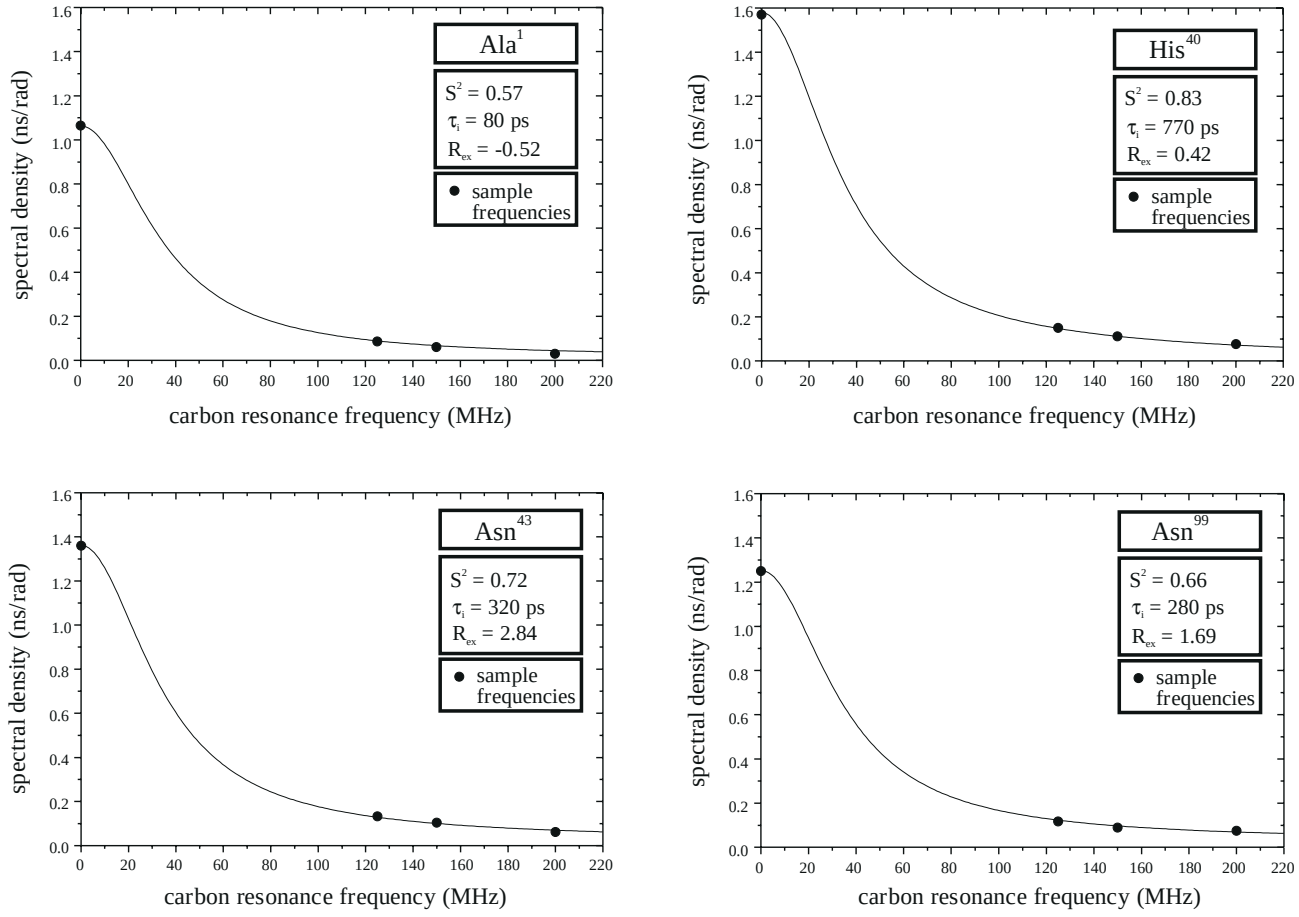

Fig. 11. Spectral density samplings for four residues as a function of frequency in MHz. The four sampling frequencies occur at 125, 150 and 200 MHz and at 3000 Hz. The spectral density function of Lipari and Szabo was fitted to the sample frequencies using the Levenberg–Marquardt algorithm.

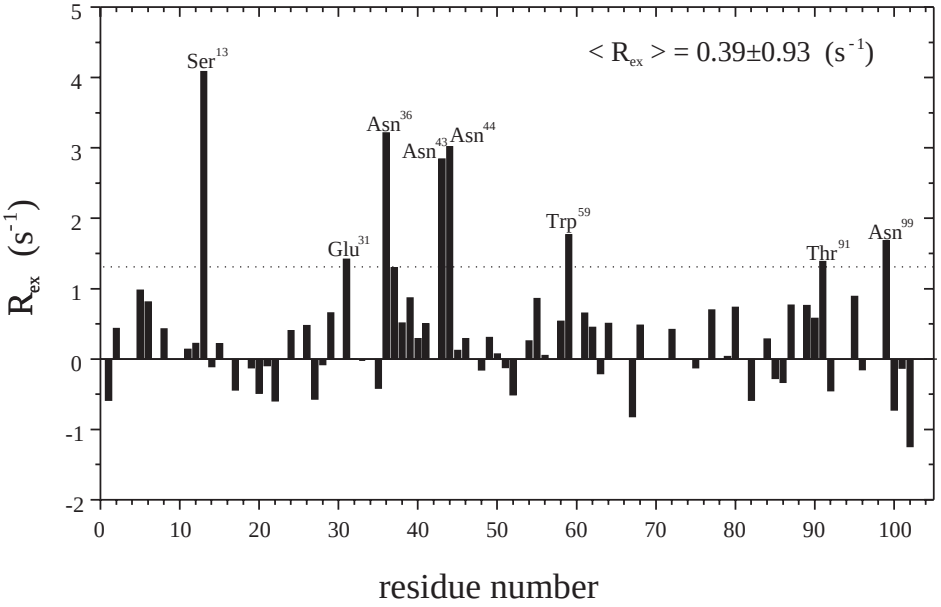

Fig. 12. Values of R_{ex} for the backbone carbonyls plotted versus the amino acid sequence.

CSA tensor for proteins in solution complicates the interpretation of the relaxation data. However, this effect can also be used as additional information: if the amplitude for the internal mobility is known from other investigations, conclusions can be drawn with respect to the anisotropy constant.

From a comparison of the order parameters $1–S^2$ derived from $^{13}C'$ and ^{15}N relaxation time measurements, a difference of 0.11 of the corresponding average values becomes apparent. This difference may be a consequence of the not exactly known values of the anisotropy constant or, as shown below, the different interpretation of the order parameters. However, the planarity of the peptide plane leads to similar order parameters for some residues: the carbonyl carbon of Asp^{49} forms a peptide plane with the amide group of Phe^{50}, and for both residues large values for $1–S^2$ were observed. The next peptide plane is more restricted, as indicated by small $1–S^2$ values for Phe^{50} ($^{13}C'$) and Ser^{51} (^{15}N). Contrary to this behaviour, the peptide plane formed by Ser^{51} ($^{13}C'$) and Val^{52} (^{15}N) is connected with larger values of $1–S^2$. In addition, the correspondence of the correlations is also obvious for the loop between Thr^{93} and Asn^{99}. This region is involved in the binding of the substrate and the competitive inhibitors of ribonuclease T1 and its increased mobility seems to be important for the activity. However, the correlation within the peptide plane cannot be confirmed for all residues. This difference of order parameters may be explained by the principal difference between the two relaxation mechanisms. Since the dominant relaxation mechanism for ^{15}N is the dipole–dipole relaxation, whereas for the carbonyl carbon it is the CSA relaxation, the interpretation of the order parameters is quite different. In the case of the dipole–dipole interaction the order parameter S^2 describes the difference of the mobility of the covalently linked $^1H^N$ and ^{15}N nuclei. Therefore, in reality, from ^{15}N relaxation time measurements one does not obtain the dynamics of the backbone nuclei but rather the motion of the $^1H^N$-^{15}N bond. The relaxation of the carbonyl carbon is caused predominantly by the CSA mechanism or, more precisely, by the motion of the CSA tensor in the static magnetic field B_0. For a rigid molecule the motion of the CSA tensor is determined by the overall correlation time τ_c and the order parameter is equal to one. Since the CSA tensor is linked to the carbonyl carbon, an additional internal flexibility of this nucleus leads to a decrease in the value of S^2. Therefore, the order parameter derived from carbonyl carbon relaxation times is a direct measure of the motion of this backbone nucleus.

In order to confirm these considerations, the internal correlation times derived from ^{15}N and $^{13}C'$ relaxation time measurements will be compared. For RNase T1 an average value of 42 ps for τ_i has been calculated using ^{15}N relaxation data. The magnitude of this value agrees well with the results from other studies, e.g. on calmodulin ($\langle\tau_i\rangle = 30$ ps, $\tau_c \approx 6.7$ ns; Barbato et al., 1992) and on FK506 binding protein ($\langle\tau_i\rangle \leq 30$ ps, $\tau_c = 9.2$ ns; Cheng et al., 1993). Contrary to these values for the internal correlation time of the carbonyl carbons, an average value of 350 ps has been obtained for τ_i from carbonyl carbon relaxation data. Even if the interpretation of τ_i is problematic, the difference of 1 order of magnitude in τ_i seems to confirm the above outlined interpretation.

Results from the second level approach

Using the second level approach, a mapping of parts of the spectral density function can be achieved for those residues for which both relaxation rates at the three dif-

ferent spectrometer frequencies 500, 600 and 800 MHz are available. In addition, this analysis provides a value for the conformational exchange parameter R_{ex}. Although the spectral densities of different models for the internal motion can be fitted to the experimental values, we applied the model of Lipari and Szabo also for this second level approach for comparison. In order to determine the overall correlation time τ_c using only the carbonyl carbon relaxation times, the well-known procedure for analysing ^{15}N relaxation times is applied: τ_c was changed stepwise assuming one value for all residues while the parameters for internal motion were fitted to the spectral density function values for each residue using a numerical optimization procedure. Finally, that value of τ_c which minimizes a target function Ψ^2 and the corresponding values for S^2 and τ_i were chosen as the best values. From this analysis a value of 4.6 ± 0.4 ns for τ_c was obtained, which agrees well with that calculated from $^{13}C^{\alpha}$ and ^{15}N relaxation times. The result of the analysis is shown for some residues in Fig. 11. The values for the conformational exchange are shown in Fig. 12. The fact that the average value of R_{ex} is not zero may be an indication that all carbonyl nuclei undergo a motion with a small amplitude on a slow time scale. But it is also possible that either further dipole–dipole interactions between $^{13}C'$ and ^{1}H have to be considered or that the anisotropy constant has to be modified for proteins in solution. However, for residues with an exchange parameter larger than the average value plus one standard deviation, a real conformational exchange may be assumed. For some of these residues (Ser^{13}, Asn^{36}, Asn^{43}) no internal parameters were obtained from the first level approach, since their T_1–T_2 combination leads to a point outside the hatched area in Fig. 7. Therefore, the dynamics of these residues can be characterized by the superposition of a fast motion in the picosecond–nanosecond range and a slow motion on the microsecond time scale. The large values of the exchange parameter of the adjacent amino acids Asn^{43} and Asn^{44} seem to be an indication for a coordinated motion of this part of the polypeptide chain. Both residues are located in the active site of the enzyme. Larger values for the exchange parameters were also derived from ^{15}N relaxation time measurements.

Conclusions

It was possible to describe the backbone dynamics of ribonuclease T1 using $^{13}C'$ relaxation measurements. Since the CSA mechanism dominates the relaxation of the carbonyl carbon, the microdynamical parameters are a direct measure for the motion of the backbone. Highly restricted motions are found for most of the secondary structure elements while the loop regions are more or less disordered and flexible. Although the internal correlation time τ_i is about 1 order of magnitude larger than that of the corresponding ^{15}N relaxation time measurements, a good agreement of the order parameters for many residues was found. However, in some cases deviations were observed, which were also observed in a similar study of Dayie and Wagner (1995). Nevertheless, the investigations of the relaxation behaviour of both nuclei are certainly useful for a better understanding of the dynamics of the protein backbone.

Acknowledgements

We thank Stefan Geschwindner and Harald Thüring for the preparation of the isotope-labelled protein sample, Matthias Haun and Michael Marek for computer technical support and Dr. David Fushman for making available software routines for fitting the relaxation data. The authors are indebted to Christian Ludwig for making available the ^{15}N order parameters. We are most grateful to Stefania Pfeiffer for helpful discussions and for providing the details of the refined solution structure of ribonuclease T1. We also thank the Deutsche Forschungsgemeinschaft for a grant (Ru145/8-7). J.E. is the recipient of a stipend from the Graduiertenkolleg 'Proteinstrukturen, Dynamik und Funktion' of the University of Frankfurt.

References

Abragam, A. (1961) *Principles of Nuclear Magnetism*, Oxford University Press, Oxford, U.K.

Barbato, G., Ikura, M., Kay, L.E., Pastor, R.W. and Bax, A. (1992) *Biochemistry*, **31**, 5269–5278.

Boyd, J., Hommel, U. and Campell, I.D. (1990) *Chem. Phys. Lett.*, **175**, 477–482.

Bronstein, I.N. and Semendjajew, K.A. (1985) *Taschenbuch der Mathematik*, 22nd ed., Verlag Harri Deutsch, Thun und Frankfurt am Main, Germany.

Bull, T.E. (1992) *Prog. NMR Spectrosc.*, **24**, 377–410.

Cheng, J.-W., Lepre, C.A., Chambers, S.P., Fulghum, J.R., Thomson, J.A. and Moore, J.M. (1993) *Biochemistry*, **32**, 9000–9010.

Clore, G.M., Driscoll, P.C., Wingfield, P.T. and Gronenborn, A.M. (1990a) *Biochemistry*, **29**, 7387–7401.

Clore, G.M., Szabo, A., Bax, A., Kay, L.E., Driscoll, P.C. and Gronenborn, A.M. (1990b) *J. Am. Chem. Soc.*, **112**, 4989–4991.

Dayie, K.T. and Wagner, G. (1995) *J. Magn. Reson.*, **B109**, 105–108.

Engelke, J. and Rüterjans, H. (1995) *J. Biomol. NMR*, **5**, 173–182.

Fogh, R.H., Schipper, D., Boelens, R. and Kaptein, R. (1995) *J. Biomol. NMR*, **5**, 259–270.

Fushman, D., Weisemann, R., Thüring, H. and Rüterjans, H. (1994) *J. Biomol. NMR*, **4**, 61–78.

Goldman, M. (1984) *J. Magn. Reson.*, **60**, 437–452.

Grzesiek, S., Döbeli, H., Gentz, R., Garotta, G., Labhardt, M. and Bax, A. (1992) *Biochemistry*, **31**, 8180–8190.

Grzesiek, S. and Bax, A. (1993) *J. Biomol. NMR*, **3**, 285–290.

Kamath, U. and Shriver, J.W. (1989) *J. Biol. Chem.*, **264**, 5586–5592.

Kay, L.E., Torchia, D.A. and Bax, A. (1989) *Biochemistry*, **28**, 8972–8979.

Kay, L.E., Ikura, M., Tschudin, R. and Bax, A. (1990) *J. Magn. Reson.*, **89**, 496–514.

Kay, L.E., Nicholson, L.K., Delaglio, F., Bax, A. and Torchia, D.A. (1992) *J. Magn. Reson.*, **97**, 359–375.
Lipari, G. and Szabo, A. (1982) *J. Am. Chem. Soc.*, **104**, 4546–4559.
Martinez-Oyanedel, J., Choe, H., Heinemann, U. and Saenger, W. (1991) *J. Mol. Biol.*, **222**, 335–352.
Peng, J.W. and Wagner, G. (1992) *J. Magn. Reson.*, **98**, 308–332.
Pfeiffer, S., Engelke, J. and Rüterjans, H. (1996) *Q. Magn. Reson. Biol. Med.*, **3**, 69–87.
Powers, R., Gronenborn, A.M., Clore, G.M. and Bax, A. (1991) *J. Magn. Reson.*, **94**, 209–213.
Press, W.H., Flannery, B.P., Teukolsky, S.A. and Vetterling, W.T. (1988) *Numerical Recipes*, Cambridge University Press, Cambridge, U.K., 1988.
Sklenář, V., Torchia, D. and Bax, A. (1987) *J. Magn. Reson.*, **73**, 375–379.
Stark, R.E., Jelinski, L.W., Ruben, D.J., Torchia, D.A. and Griffin, R.G. (1983) *J. Magn. Reson.*, **55**, 266–273.
Yamazaki, T., Yoshida, M. and Nagayama, K. (1993) *Biochemistry*, **32**, 5656–5669.
Yamazaki, T., Muhandiram, R. and Kay, L.E. (1994) *J. Am. Chem. Soc.*, **116**, 8266–8278.
Ye, C., Fu, R., Hu, J., Hou, L. and Ding, S. (1993) *Magn. Reson. Chem.*, **31**, 699–704.
Zeng, L., Fischer, M.W.F. and Zuiderweg, E.R.P. (1996) *J. Biomol. NMR*, **7**, 157–162

Appendix

Substituting the expressions for the spectral density function of the carbonyl carbon and of the $^{13}C'$-$^{13}C^{\alpha}$ interaction into Eqs. 6a and 6b, one obtains

$$\frac{1}{T_1} - \rho^1_{C'C^\alpha} - \rho^1_{cross} = d^2_{CSA}\omega^2_C \frac{2}{5}\left[\frac{S^2\tau_c}{1+\omega^2_C\tau^2_c} + \frac{(1-S^2)\tau_i}{1+\omega^2_C\tau^2_i}\right] \quad (A1)$$

$$\frac{1}{T_2} - \rho^2_{DD} - \rho^2_{cross} = d^2_{CSA}\omega^2_C \times\left[\frac{4}{15}\left(S^2\tau_c + (1-S^2)\tau_i\right) + \frac{1}{2d^2_{CSA}\omega^2_C}\left(\frac{1}{T_1} - \rho^1_{C'C^\alpha} - \rho^1_{cross}\right)\right] \quad (A2)$$

From Eq. A2, S^2 as a function of τ_i can be derived:

$$S^2 = \frac{1}{\tau_c - \tau_i}\left[\frac{15}{8d^2_{CSA}\omega^2_C}\underbrace{\left(\frac{2}{T_2} - 2\rho^2_{DD} - 2\rho^2_{cross} - \left(\frac{1}{T_1} - \rho^1_{C'C^\alpha} - \rho^1_{cross}\right)\right)}_{A} - \tau_i\right] = \frac{1}{\tau_c - \tau_i}(A - \tau_i) \quad (A3)$$

'A' depends only on the measured relaxation rates and the values for $\rho_{C'C^\alpha}(\tau_c)$ and ρ_{cross}, which are known for a given overall correlation time τ_c. When this expression is substituted back into Eq. A1, a relation for the effective internal correlation time is achieved which depends only on T_1 and T_2. Unfortunately, this equation is of third order in τ_i:

$$\left(\frac{B(1+\omega^2_C\tau^2_c)}{\tau_c} - 1\right)\tau^3_i + \left(A - B(1+\omega^2_C\tau^2_c)\right)\tau^2_i + \frac{1}{\omega^2_C}\left(\frac{B-A}{\tau_c}(1+\omega^2_C\tau^2_c) + \omega^2_C\tau^2_c\right)\tau_i + \frac{1}{\omega^2_C}\left(A - B(1+\omega^2_C\tau^2_c)\right) = 0 \quad (A4)$$

with $B = (5/2d^2_{CSA}\omega^2_C)((1/T_1) - \rho^1_{C'C^\alpha} - \rho^1_{cross})$. In order to arrive at a solution for τ_i the formalism of Cardano (Bronstein and Semendjajew, 1985) can be used, but this treatment is difficult and time-consuming. Because of the symmetry of the spectral density function of $^{13}C'$, the first solution can be assumed to be $\tau_{i,1} = \tau_c$. Then a polynomial division leads to an equation of second order in τ_i and its solutions are given by Eqs. 8b and 8c.